Low-cost Optical Wireless CDMA Transceiver Design for IoT Applications

Gregory Dzhezyan†, Hovannes Kulhandjian†, Michel Kulhandjian‡, and Michael Rahaim††
†Department of Electrical and Computer Engineering, California State University, Fresno, Fresno, CA 93740, U.S.A.
E-mail: {gregorydz,hkulhandjian}@mail.fresnostate.edu
‡Department of Electrical and Computer Engineering, Rice University, Houston, TX, 77005, U.S.A.
E-mail: michel.kulhandjian@rice.edu
††Department of Engineering, University of Massachusetts at Boston, Boston, MA, 02125 U.S.A.
E-mail: Michael.Rahaim@umb.edu

2023 IEEE Latin-American Conference on Communications (LATINCOM) | 979-8-3503-2687-1/23/$31.00 ©2023 IEEE | DOI: 10.1109/LATINCOM59467.2023.10361875

***Abstract*—In this work, we implement a low-cost optical wireless communication (OWC) system based on code-division multiple access (CDMA). The system can be used in Internet of Things (IoT) applications as it is low-cost and can easily be deployed in small IoT devices. Due to the line-of-sight nature of OWC, the system provides a secure communication means. The framework uses white light LEDs for transmission and an array of 9 photodiodes for reception. Pulsed on-off-keying (OOK) modulation is used with CDMA applied for multi-user scenarios. Each user in a CDMA network is assigned a unique code. Two users modulate their signals using the CDMA codes which are jointly transmitted from a single transmitter to multiple receivers. Many formulations exist for generating these unique codes, however, in this work, we use a very popular set of codes called Walsh codes (also known as Hadamard matrices).**

***Index Terms*—Visible Light Communication (VLC), Optical Wireless Communication (OWC), Code Division Multiple Access (CDMA), On-Off Keying (OOK), Low-cost Receiver.**

I. Introduction

Visible light communication (VLC) is a wireless optical communication technology that uses the visible light spectrum to transmit data. VLC is an optical wireless communication (OWC) technique in the visible band, while OWC also includes the infrared (IR) band. VLC and OWC have gained interest from the research community during the past two decades. Code-division multiple access (CDMA) is a direct-sequence spread spectrum (DSSS) technique that trades bandwidth for reduced signal interference, making it possible to communicate even under the noise floor [1]. These properties make CDMA a potentially advantageous candidate communication scheme for multi-user VLC systems.

Applications for VLC systems include uses in the transportation industry to augment traffic lights and vehicle headlights. For example in [2], [3] a low-cost receiver is designed for integration into a typical stop light. In [4] a more thorough discussion is carried out on the applications of VLC for traffic communication including intra-vehicular and infrastructure-to-vehicle communications. VLC can also be used for indoor applications. In [5] an analysis is carried out for indoor channel characteristics and in [6] an indoor positioning system based on VLC using triangulation is proposed. Le-Minh *et al.* [7] developed a short-range visible light communications system using blue, green, and red LEDs. Similarly, a low-cost front-end receiver for short-range, broadband wireless applications is conceived by Joyner *et al.* [8]. It could also be used for software-defined radio (SDR)-based optical wireless communications (OWC) applications, as discussed in [9].

979-8-3503-2687-1/23/$31.00 ©2023 IEEE

In our previous research work in [2], [3], we utilized two photodiodes at the receiver and had a simple BPSK modulation scheme. In our current work, we propose and implement a low-cost OWC system based on CDMA, which allows multiple users to transmit information at the same time synchronously. In addition to that, we make use of a 3×3 array of photodiode receivers, which significantly enhances the system's reception capabilities, thereby extending its communication range compared to our previous work. The system utilizes on-off keying (OOK) to modulate a white light-emitting diode (LED) to achieve the transmission of information. The receivers in this system are composed of an array of 9 photodiodes that translate the pulses of light into a current. Experiments were carried out in the lab to test the robustness of the proposed system.

The rest of the paper is organized as follows. In Section II, we present the design methodology, followed by the CDMA modulation in Section III. In Section IV, we discuss the experimental results and analysis before presenting our conclusion and future work in Section V.

II. Design Methodology

In this section, we delve into the hardware design of the optical wireless transmitters and receivers within the test system.

A. Transmitter

In this system, the transmitter consists of a high-power LED that operates in an on-off fashion. It is modulated by a pseudo-random square wave input, which carries the information bits for transmission. The circuitry is composed of a Darlington pair configuration, as shown in Fig. 1, to drive the high-power LED. High-power LEDs can be run from low voltage levels (e.g., $V_{dd} = 5V$) as long as enough current is supplied. In the Darlington pair configuration, two BJT devices are interconnected to function as a single

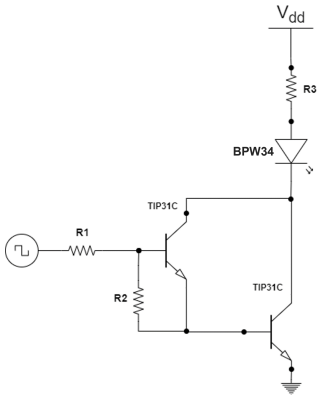

Fig. 1: Transmitter circuit design.

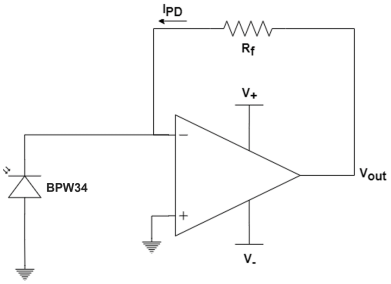

Fig. 2: A photovoltaic mode transimpedance amplifier.

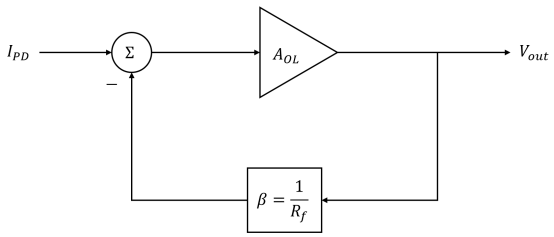

Fig. 3: Block diagram of a photovoltaic mode transimpedance amplifier.

transistor with significantly enhanced current amplification capabilities. The current gain of the pair is the product of the individual gains for each device [10]. Therefore, this design is well-suited for modulating the high-power LED's on-and-off operation. Note that in the design, R_3 is a current limiting resistor for the LED, and can be used to set the maximum brightness of the LED on the state ($R_3 = 20\Omega$ was used.) The rest of the resistors were chosen as $R_1 = 500\Omega$ and $R_2 = 100k\Omega$, similar to our former design configuration [2].

A National Instruments DAQ unit is employed to interface the transmitter circuit in Fig. 1, serving as the input for the square wave/pulse train that carries the information for transmission.

B. Receiver

The receiver design involves the use of a transimpedance amplifier (TIA). However, care must be taken in TIA design since there is a tendency for these circuits to become unstable, particularly for high-speed applications involving photodiodes. This instability is due to the parasitic effects of the photodiode and amplifier used. Figure 2 shows a photodiode connected to an amplifier in what is known as photovoltaic mode. If a reverse bias is applied to the photodiode (i.e., negative voltage applied to the anode) a photoconductive configuration will result. In a photoconductive configuration, the depletion region of the photodiode increases in size, making the device more sensitive, reducing its capacitance, and pushing back the photo-current saturation point with regard to illuminance (extending the linear region of operation). Reverse biasing also increases the dark current, the level of current produced by the diode under zero illuminance. Hence, photovoltaic mode is favorable for low-illuminance settings and photoconductive for high-illuminance scenarios. The photoconductive mode may also aid in stabilizing the circuit due to the reduction in the diode's parasitic capacitance; therefore, photoconductive mode was chosen in our design [10], [11].

In Fig. 2 the photodiode can be viewed as being connected in between the input terminals of the op-amp. Since the non-inverting input is grounded, and if the op-amp is assumed to be ideal, then the inverting input will also be at the ground voltage level (i.e., 0V across the diode). In this configuration, when a photon is incident on the active area of the diode a photocurrent, I_{PD}, flows from the cathode to the anode. When the current flows through the feedback resistor R_f, a voltage, V_{out}, is produced. It is possible to derive the closed-loop transfer function for the circuit shown by drawing the block diagram, as shown in Fig. 3, [10], [12].

In Fig. 3, A_{OL} is the open loop gain for a given amplifier and is generally frequency dependent ($A_{OL}\,(j\omega)$). The closed-loop transfer function or gain is obtained by reducing the block diagram,

$$\frac{V_{out}}{I_{PD}} = \frac{A_{OL}}{1 + \beta A_{OL}}. \tag{1}$$

The open loop gain for an amplifier, A_{OL}, is typically very large, therefore the loop gain $\beta A_{OL} \gg 1$, and we have that

$$\frac{V_{out}}{I_{PD}} = \frac{A_{OL}}{1 + \beta A_{OL}} \approx \frac{A_{OL}}{\beta A_{OL}} = \frac{1}{\beta}. \tag{2}$$

Hence, the closed loop transfer function can be approximated as $\frac{1}{\beta}$. For the TIA circuit in Fig. 2, $\beta = \frac{1}{R_f}$. Therefore, the transfer function of the basic TIA circuit is given by

$$\frac{V_{out}}{I_{PD}} = R_f. \tag{3}$$

Note that in (3) the gain is in terms of Volts/Amp (transimpedance gain V/A) and not Volt/Volt (voltage gain V/V). The transimpedance gain can, in general, be much higher than the voltage gain, [10], [12].

The closed-loop transfer function of (3) is the signal gain of the op-amp. The noise gain is derived by imagining a small voltage source connected to the non-inverting input of the op-amp. When the noise gain transfer function is derived while

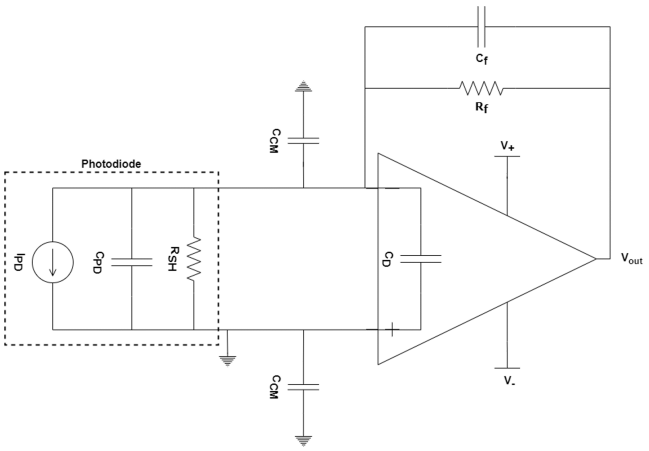

Fig. 4: Equivlenat model of the photodiode and an amplifier showing its parasitic components.

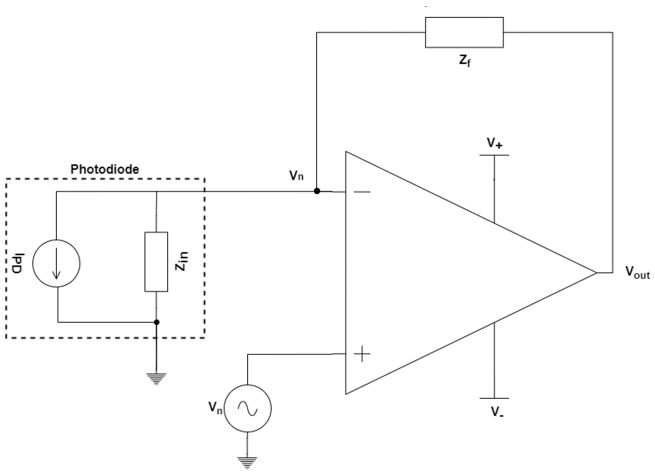

Fig. 5: TIA circuit model for deriving the noise gain transfer function.

considering the photodiode's parasitic capacitance, one will see a single pole-zero structure in the system. This pole's frequency is far smaller than the zero's for the circuit of Fig. 2. To counteract this, a feedback capacitor is added to the circuit to better control the pole location, allowing us to attenuate noise and maintain the same signal gain, [10]–[12].

In Fig. 4, the photodiode has been expanded into its equivalent model where a current source, I_{pd}, represents the current produced by incident light usually on the order microamps, C_{PD}, a parasitic capacitance on the order of picofarads, and shunt resistance, R_{SH}, on the order of gigaohms. Additionally shown is the parasitic common mode capacitance, C_{CM}, of the inverting and non-inverting inputs, and the parasitic differential capacitance, C_D, of the amplifier, [11].

An analysis of this circuit begins by realizing that the common-mode capacitor, C_{CM}, at the non-inverting input is connected between ground and ground, and therefore can be eliminated. Then, observe that the remaining capacitors, except for C_f, are in parallel and can be summed as

$$C_{in} = C_{PD} + C_{CM} + C_D. \tag{4}$$

Now this total input capacitance can be combined with the resistor R_{SH} into a total input impedance, Z_{in}. The same can be done for the feedback components to form a total feedback impedance, Z_f

$$Z_{in} = \frac{R_{SH}}{C_{in}R_{SH}s + 1}, \tag{5}$$

$$Z_f = \frac{R_f}{C_f R_f s + 1}. \tag{6}$$

These new impedances are shown in Fig. 5, where the circuit from Fig. 4 has been redrawn with an additional noise voltage source, V_n, at the non-inverting input of the op-amp. If the ideal op-amp assumptions are held, note that V_n will also be present at the inverting input. From the new circuit in Fig. 5, it is possible to describe V_n at the inverting input as a voltage division from V_{out} to ground as follows,

$$V_n = \frac{Z_{in}}{Z_{in} + Z_f} V_{out}. \tag{7}$$

Now, realize that $\beta^* = \frac{Z_{in}}{Z_{in}+Z_f}$, and the closed-loop transfer function can be determined by $\frac{1}{\beta}$ as

$$\frac{1}{\beta} = \frac{Z_{in} + Z_f}{Z_{in}}. \tag{8}$$

We can expand (8) using (5) and (6) to determine the noise gain transfer in terms of the individual discrete components as such,

$$\frac{Z_{in} + Z_f}{Z_{in}} = \frac{R_f R_{SH}\left(C_f + C_{in}\right)s + R_{SH} + R_f}{R_{SH}\left(C_f R_f s + 1\right)}. \tag{9}$$

Finally, from (9) the closed-loop noise gain transfer function for the TIA circuit in Fig. 4 is given by

$$G_{noise}(s) = \frac{R_f + R_{SH}}{R_{SH}} \frac{\frac{R_f R_{SH}}{R_f + R_{SH}}\left(C_f + C_{in}\right)s + 1}{C_f R_f s + 1}. \tag{10}$$

The signal gain of the same circuit is now expressed by

$$G_{signal}(s) = Z_f = \frac{R_f}{C_f R_f s + 1}. \tag{11}$$

From the noise gain transfer function in (10), we can determine the zero and pole frequencies as

$$f_p = \frac{1}{2\pi R_f C_f}, \tag{12}$$

$$f_z = \frac{1}{2\pi \frac{R_f R_{SH}}{R_f + R_{SH}}\left(C_f + C_{in}\right)}. \tag{13}$$

The design of the TIA is informed by the maximum photocurrent for the BPW34 photodiode. This value is approximately 70 microamps. To obtain an output of the TIA, V_{out}, to be 5V when this max current is produced, then using (3) results in $R_f \approx 71k\Omega$.

*Note that feedback transfer function, β, is for the circuit in Fig. 5 which is unitless and is different from the previous β in (2).

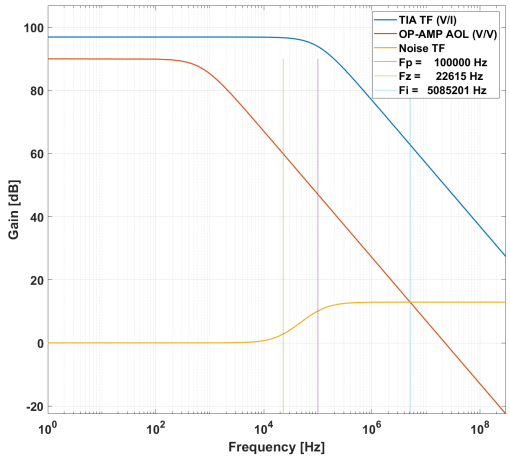

Fig. 6: A plot of the noise gain and signal transfer functions. Additionally plotted is the estimated amplifier open-loop gain curve.

Using the determined resistor value R_f, we determine C_f by choosing a pole frequency f_p and solving (12). The value chosen for f_p is ultimately determined by the bandwidth of the TIA circuit. The frequency of the pole, f_p, is chosen such that it is smaller than the amplifier's unity gain bandwidth product (GBWP), but more importantly, that it cancels the zero f_z before the noise gain transfer function intercepts the amplifier's open loop gain curve. Figure 6 shows an example of the noise gain curve (yellow) plotted against the amplifier's open-loop curve (red). The pole f_p location was set to be at $\frac{GBWP}{1000}$ and is shown on Fig. 6 (purple vertical line). Note that for the amplifier $GBWP = 100MHz$ was used.

From Fig. 6 it can be seen how the pole is at just the appropriate location to cause the noise gain to level out before it intersects the amplifier's open-loop gain curve. This is important because the rate-of-closure (ROC) between these two curves determines the phase margin ϕ_m of the system. The goal is to have a phase margin $\phi_m < 180°$. The ROC (calculated at the intercept frequency $\omega_i = 2\pi f_i$) is defined by

$$ROC = Slope\left(|G_{noise}(j\omega_i)|\right) - Slope\left(|A_{OL}(j\omega_i)|\right), \quad (14)$$

where the slope is in dB/dec unit. Using ROC, the phase margin ϕ_m can be approximated by

$$\phi_m \approx 180° - 4.5 * ROC. \quad (15)$$

From Fig. 6, the $ROC \approx +20$ dB/dec and $\phi_m \approx 90°$. However, the phase margin ϕ_m can be more accurately determined if the intercept frequency f_i is known. Figure 6 also shows the intercept frequency of the noise gain curve with the amplifier's open-loop gain curve (light blue vertical line). For a more accurate phase margin estimate, let

$$T(j\omega) = A_{OL}(j\omega) - G_{noise}(j\omega). \quad (16)$$

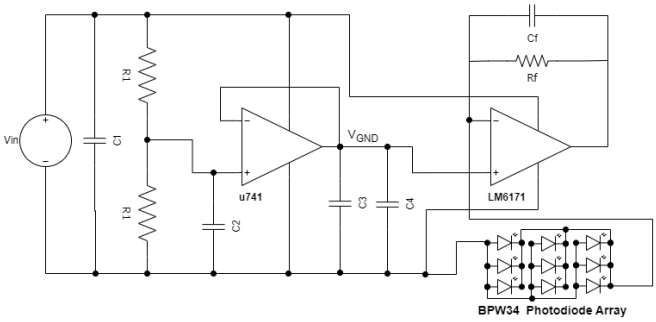

Fig. 7: Final design of the receiver. The u741 op-amp is acting as rail-splitter and LM6171 is the TIA.

Now determine the phase margin by

$$\phi_m = 180° + tan^{-1}\left(T(j2\pi f_i)\right). \quad (17)$$

Phase margin can also be determined analytically by estimating the amplifier's open-loop response curve $A_{OL}(j\omega)$ from its datasheet using a first-order transfer function as in (19). Then evaluating the limit as $s \to \infty$ for the noise gain transfer function, as shown in (18). Finally, equating those two quantities we obtain

$$\lim_{s\to\infty} \frac{R_f + R_{SH}}{R_{SH}} \frac{\frac{R_f R_{SH}}{R_f + R_{SH}}\left(C_f + C_{in}\right)s + 1}{C_f R_f s + 1} = \frac{C_f + C_{in}}{C_f}, \quad (18)$$

$$A_{OL}(s) \approx \frac{A_{OL} * f_{knee}}{s + f_{knee}}. \quad (19)$$

The final design of the system is shown in Fig. 7.

After some experimentation in the lab the final values for the TIA feedback resistor R_f was chosen to be $70k\Omega$ and the feedback capacitor C_f was chosen to be $15pF$. In the design the capacitors, C_1, C_2, C_3, C_4 are decoupling and bypass capacitors whose values are $10\mu F$, $0.001\mu F$, $0.01\mu F$, and $10\mu F$, respectively were used. The resistor R1 is $10k\Omega$ and V_{in} should not exceed 15V. The voltage divider formed by R1 is used to evenly split the input voltage. The u741 is in voltage follower configuration sampling the midpoint of the voltage divider and providing a virtual ground to the rest of the circuitry. By applying 10V to V_{in} this ensures that LM6171 receives +5V and -5V on its input rails. This additionally causes the photodiode array to be reverse biased with -5V applied to the anode.

III. CDMA Modulation

In this section, we describe the implementation of the CDMA scheme for the optical domain.

A CDMA network enables multi-user communication by assigning unique codewords to each user on the system. These codewords are determined mathematically using Hadamard matrices. The process for generating these codes is described in (20 - 22), [13]

$$H_1 = \begin{bmatrix} 1 \end{bmatrix}, \tag{20}$$

$$H_2 = \begin{bmatrix} 1 & 1 \\ 1 & -1 \end{bmatrix}, \tag{21}$$

$$H_{2^n} = \begin{bmatrix} H_{2^{n-1}} & H_{2^{n-1}} \\ H_{2^{n-1}} & -H_{2^{n-1}} \end{bmatrix}, \tag{22}$$

where n represents the number of users in the network [14]. This process of codeword generation causes each row vector of the matrix to be orthogonal to one another (i.e., $r_i \cdot r_j = 0$ for $i \neq j$). By exploiting this orthogonality property, CDMA encodes the messages of multiple users on the system into a single transmission. This is done by spreading each user's message with their uniquely assigned code and then summing over all users on the system. Users can then recover messages intended for them by convolving the appropriate code with the total received signal. Note that as the number of users, n, grows, the size of the Hadamard matrix increases exponentially as does the length of the codewords. Additionally, the summing of the spread messages will cause the final message to have values in the range 2^n to -2^n.

In the system implemented here, a sequence of M random bits is generated and converted into binary phase-shift keying (BPSK) symbols. The BPSK symbol stream is spread with a Walsh code by replacing each symbol by the code with the sign of the symbol distrusted through the code. An example of this procedure is shown in Fig. 8, where each user has a length 4 messages for transmission. Note that the message has already been converted to BPSK symbols. Each user is additionally assigned a code from the first two rows of the H_4 Hadamard matrix. The message for each user is spread, summed together, and finally converted to the bit stream that will modulate the transmitter LED.

These two's complement encoding scheme of the final CDMA message will further impact our data rate, as the binary expansion of the CDMA symbols is also dependent on the number of users on the system. For a constant OOK transmit frequency f_{tx}. Let L be the code length of a user, M the average length of a message, and B the bit-width used for expansion. Then the message duration in time, and

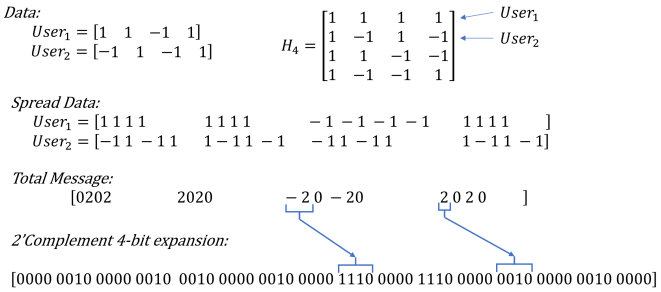

Fig. 8: An example of a transmission for two users in our optical CDMA network.

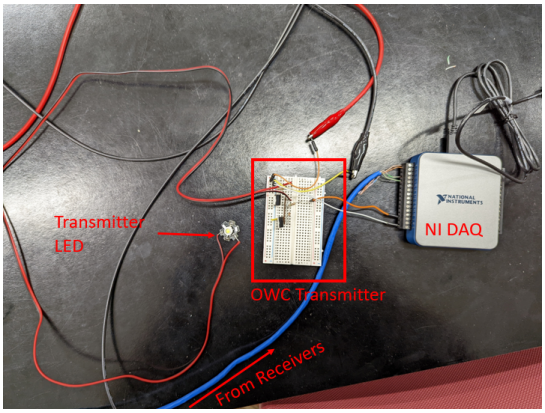

Fig. 9: The OWC transmitter circuit.

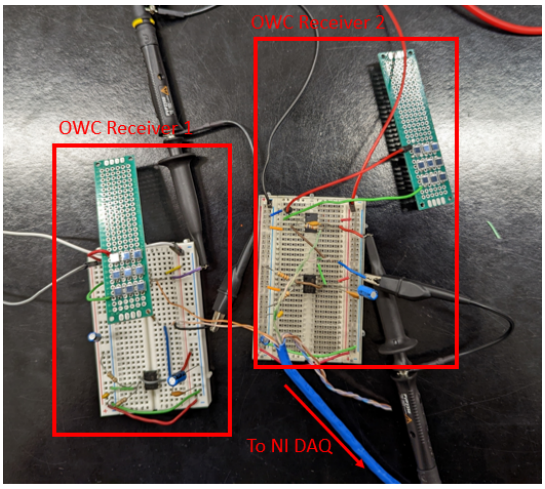

Fig. 10: The two OWC receiver circuits.

therefore the time to transmit is given by:

$$t_{msg} = \frac{LMB}{f_{tx}}. \tag{23}$$

IV. Experimental Results

An experiment was conducted in a laboratory where two different messages, each of 1000 random bits, are transmitted using one OWC transmitter. The distance between the transmitter and receiver was about one meter. Additionally, the ambient light in the room was at a fairly low level at the time of transmission. The transmission, with both messages encoded in the signal, is received successfully by two OWC receivers. Each message is intended for a specific receiver based on the Walsh code they are assigned.

Figure 9 shows the transmitter with all the hardware connected to the NI DAQ. The NI DAQ is connected to a laptop computer running MATLAB software. Figure 10 shows the two optical OWC receiver circuits with their own photodiode 3×3 array. Figure 11 shows an example of a recorded waveform from one of the receivers. The overlaid orange waveform is the result of thresholding the received

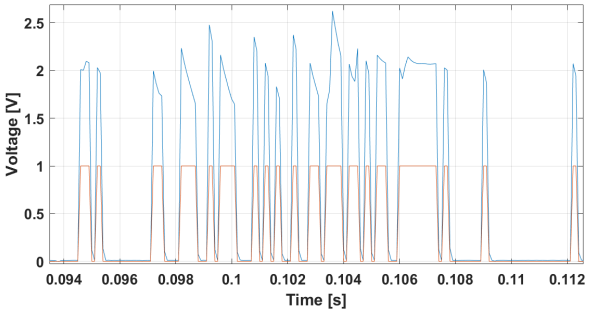

Fig. 11: An example of a received signal in blue. The orange curve is the result of thresholding the blue curve.

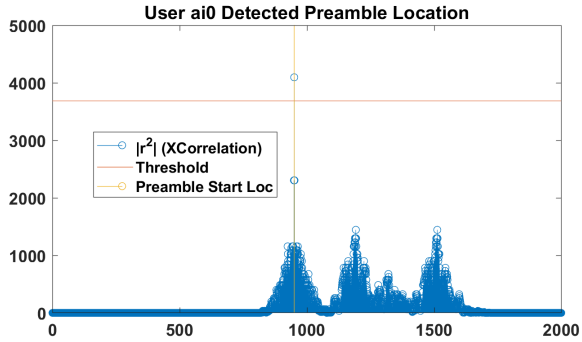

Fig. 12: Preamble detection code output.

waveform around its average value, (max-min)/2. The system uses a preamble inserted at the beginning of the transmission to detect the start of a message to the receivers. The preamble used in hexadecimal is [0xAC, 0xDD, 0xA4, 0xE2, 0xF2, 0x8C, 0x20, 0xFC].

The preamble detector uses cross-correlation to determine its location within the sampled time stream of voltages. A threshold is computed based on a user-supplied parameter in the range [0,1], and the magnitude squared maximum value of the preamble auto-correlation. The output of the preamble detector is shown in Fig. 12, the threshold value is the red vertical line and a stem in yellow has been placed where it is believed the preamble starts. Once the preamble has been detected, it is simply a matter of downsampling the thresholded received waveform by the ratio of the receiver sample rate to the transmitter sample rate, and then performing the procedure shown in Fig. 8 in reverse to demodulate and decode the data bits.

V. Conclusion and Future Work

In this work, an optical CDMA communication system was implemented and tested. Physical circuitry was designed for both the transmitter and the receivers. The software was developed in MATLAB using NI DAQ units to control all hardware. Finally, an experiment was successfully conducted using one transmitter and two receivers. The experiment involved the transmission of messages with random bit information, each intended for specific users within the network.

The two's complement encoding scheme presented in this work is not very efficient. An investigation into other encoding schemes should be conducted to further improve the system. A potential alternative scheme worthy of investigation is the 8b/10b high-speed line codes. 8b/10b codes are typically found in high-speed communication links such as fiber optics, universal serial bus (USB), and peripheral component interconnect express (PCIe).

Acknowledgement

Student research funding for this effort was provided by Edison International through the Lyles College of Engineering Research Grant.

References

[1] Y. Qiu, S. Chen, H.-H. Chen, and W. Meng, "Visible Light Communications Based on CDMA Technology," *IEEE Wireless Communications*, vol. 25, no. 2, pp. 178–185, 2018.

[2] W. Greives and H. Kulhandjian, "Design and Experimentation of a Low-cost Receiver for Visible Light Communications," in *2020 IEEE Latin-American Conference on Communications (LATINCOM)*, 2020, pp. 1–6.

[3] H. Kulhandjian, W. Greives, and M. Kulhandjian, "Smart Traffic Light Controller using Visible Light Communications," in *2022 IEEE Vehicle Power and Propulsion Conference (VPPC)*, 2022, pp. 1–6.

[4] A. Memedi and F. Dressler, "Vehicular Visible Light Communications: A Survey," *IEEE Communications Surveys and Tutorials*, vol. 23, no. 1, pp. 161–181, 2021.

[5] K. Lee, H. Park, and J. R. Barry, "Indoor Channel Characteristics for Visible Light Communications," *IEEE Communications Letters*, vol. 15, no. 2, pp. 217–219, 2011.

[6] J. Luo, L. Fan, and H. Li, "Indoor Positioning Systems Based on Visible Light Communication: State of the Art," *IEEE Communications Surveys & Tutorials*, vol. 19, no. 4, pp. 2871–2893, 2017.

[7] H. Le-Minh, L. Zeng, D. O'Brien, O. Bouchet, S. Randel, J. Walewski, J. Borges, K. Langer, J. Grubor, K. Lee *et al.*, "Short-range visible light communications," in *Proceedings of the Wireless World Research Forum, Chenai, Indian*, 2007.

[8] V. M. Joyner, S. Harris, and S. Sonkusale, "On the Design of Low-Power Front-End Receiver Circuits for Broadband Optical Free-Space Links," in *IFIP Int. Conf. on Wireless and Optical Commun. Networks (WOCN)*, 2007, pp. 1–4.

[9] A. Ahmed, G. Dzhezyan, H. Aboutahoun, V. Chu, J. DiViccaro, V. Ohanian, S. Rezaeiboroujerdi, I. Saheb, E. Urban, J. Wu *et al.*, "SDR Beyond Radio: An OOT GNU Radio Library for Simulation and Deployment of Multi-Cell/Multi-User Optical Wireless Communication Systems," in *Proceedings of the GNU Radio Conference*, vol. 7, no. 1, 2022.

[10] D. A. Neamen and D. A. Neamen, *Microelectronics: Circuit analysis and design*. McGraw-Hill, 2007.

[11] J. G. Graeme, *Photodiode amplifiers: OP AMP solutions*. McGraw-Hill, 1996.

[12] J. W. Nilsson and S. A. Riedel, *Electric Circuits*. Prentice Hall, 2008.

[13] M. Kulhandjian, H. Kulhandjian, and C. D'Amours, "Code design for noncoherent detection in satellite communication systems," in *2020 International Wireless Communications and Mobile Computing (IWCMC)*. IEEE, 2020, pp. 52–56.

[14] J. G. Proakis and M. Salehi, *Communication Systems Engineering*. USA: Prentice-Hall, Inc., 1994.